Biosensors and Bioelectronics 26 (2011) 3627–3632

Contents lists available at ScienceDirect

Biosensors and Bioelectronics

journal homepage: www.elsevier.com/locate/bios

Graphene-assisted dual amplification strategy for the fabrication of sensitive amperometric immunosensor

Kunping Liu[a,b], Jing-Jing Zhang[a], Chunming Wang[b,*], Jun-Jie Zhu[a,*]

[a] Key Lab of Analytical Chemistry for Life Science (MOE), School of Chemistry and Chemical Engineering, Nanjing University, Nanjing 210093, PR China
[b] School of Chemistry and Chemical Engineering, Lanzhou University, Lanzhou 730000, PR China

ARTICLE INFO

Article history:
Received 1 December 2010
Received in revised form 28 January 2011
Accepted 12 February 2011
Available online 19 February 2011

Keywords:
Graphene
Gold nanoparticle
Electrochemical immunosensor
Signal amplification

ABSTRACT

A sensitive electrochemical immunosensor with graphene-assisted signal amplification has been developed. In order to construct the base of the immunosensor, a novel hybrid architecture was initially fabricated by combining poly (diallyldimethylammonium chloride) functionalized graphene nanosheets (PDDA-G) and gold nanoparticles (AuNPs) via a simple sonication-induced assembly. The formed hybrid architecture provided an effective matrix for antibody immobilization with good stability and bioactivity. Subsequently, a smart, multilabel, and graphene-based nanoprobe that contains gold nanoparticles functionalized exfoliated graphene oxide and horseradish peroxidase-secondary antibodies was designed for constructing a novel sandwiched electrochemical immunosensor. Enhanced sensitivity was obtained by combining the advantages of high-binding capability and excellent electrical conductivity of hybrid architecture with the multilabel signal amplification. On the basis of the dual signal amplification strategy of graphene-based architecture and the multilabel, the immunosensor displayed excellent analytical performance for the detection of human IgG (HIgG) range from 0.1 to 200 ng/mL with a detection limit of 0.05 ng/mL at 3σ. Moreover, the proposed method showed good precision, acceptable stability and reproducibility, and could be used for the detection of HIgG in real samples. Therefore, the present strategy definitely paves a way for the wide application of graphene in clinical research.

1. Introduction

The immunoassay, based on the highly specific antibody–antigen recognition, has been widely used in the sensitive quantitative detection of disease-related proteins which was critical for many biomedical research and diagnostics (Bilitewski, 2000; Van Emon and Lopez-Avila, 1992). Compared with conventional immunoassays such as enzyme-linked immunosorbent assay (ELISA) and chemiluminescence immunoassay (Kato and Shimizu, 1986; Lin et al., 2004), electrochemical immunoassay has attracted considerable interest in wide range for its intrinsic advantages such as high sensitivity, low cost and fast analysis (Tang et al., 2010; Zhang et al., 2009; Li et al., 2006; Wang, 2006). In recent years, with the development of nanoscience and nanotechnology, a variety of nanoparticles, such as carbon nanotube, carbon sphere and gold nanoparticles, have been applied as the labels in nanoparticle-based amplification platforms which can dramatically enhance the signal intensity of electrochemical immunosensor and lead to ultrasensitive bioassays (Yu et al., 2006; Cui et al., 2008a; Wu et al., 2009). Although great achievement has been obtained in this field, it was still a challenge for the fabrication of novel immunosensors using new materials to achieve sensitive, fast and facile detection.

Graphene, a single layer of carbon atoms in a closely packed honeycomb two-dimensional lattice, has recently attracted enormous attention in constructing electrochemical biosensors due to its novel properties such as good mechanical strength, zero band gap, high carrier mobility, large specific surface area and outstanding electric conductivity (Xia et al., 2010; Li et al., 2008; Geim and Novoselov, 2007; Novoselov et al., 2005). For example, Du et al. (2010a) has developed a sensitive electrochemical immunosensor using chitosan/graphene composite as the substrate material for immunodetection of α-fetoprotein antigen. Wei et al. (2010) has achieved sensitive detection of norethisterone antigen using thionine/graphene based electrochemical immunosensor. However, the poor biocompatibility of graphene limits their further application in designing biosensors because graphene is hydrophobic and tends to form agglomerates in water (Shan et al., 2009a). Therefore, covalent or noncovalent functionalization methods, such as using polymers or DNA as the functionalization agent, have been made to improve the biocompatibility of graphene (Stankovich et al., 2006; Lv et al., 2010). Among them, the positive poly (diallyldimethylammonium chloride) (PDDA) functionalized graphene (PDDA-G) reported in our previous work (Liu et al., 2010) exhib-

* Corresponding authors. Tel.: +86 25 83597204; fax: +86 25 83597204.
E-mail addresses: wangcm@lzu.edu.cn (C. Wang), jjzhu@nju.edu.cn (J.-J. Zhu).

0956-5663/$ – see front matter © 2011 Elsevier B.V. All rights reserved.
doi:10.1016/j.bios.2011.02.018

ited good conductivity, solubility and biocompatibility and thus can be modified by the negative gold nanoparticles (AuNPs) for the formation of AuNPs/PDDA-G hybrid architecture. The hybrid architecture can be an ideal substrate material to provide a biocompatible microenvironment for the immobilization of antibody as well as retaining native bioactivity due to the good affinity of AuNPs for biomolecules. Meanwhile, it can also accelerate the electron transfer on the electrode surface to amplify the electrochemical signal due to the outstanding electric conductivity.

On the other hand, the detection signal of the conventional sandwich-type electrochemical enzyme immunoassays usually derived from the labeled enzyme conjugated with secondary antibodies. To increase the efficiency and sensitivity of the immunosensor, much attention is paid to the development of novel nanomaterials as labels, including metal nanoparticles, quantum dots and carbon nanotubes (Hansen et al., 2006; Rijiravanich et al., 2008). Recently, exfoliated graphene oxide (EGO) has been widely used in drug loading and delivery, optical and fluorescent DNA detection (Liu et al., 2008; Du et al., 2010b), owing to its large specific surface area (two accessible sides), abundant oxygen functional groups and high water solubility (Dreyer et al., 2010). However, the electric conductivity of EGO is much lower than reduced graphene, which limits its application in electrochemical immunosensor. On the contrary, gold nanoparticles have been well recognized as biocompatible and conductive labels for electrochemical signal amplification. Therefore, the combination of EGO with gold nanoparticles as labels should be beneficial to develop highly sensitive immunosensors.

In this work, a novel AuNPs/PDDA-G hybrid architecture with good electric conductivity and biocompatibility was fabricated via a simple sonication-induced assembly. The formed architecture could provide an effective matrix for antibody immobilization with good stability and bioactivity. Subsequently, by a layer-by-layer assemble technique, a multilabel-antibody functionalized EGO composite nanoprobe was obtained and used as labels for the construction of a novel sandwich electrochemical immunosensor. Due to the high enzyme loading capacity on EGO bioconjugate label and the upstanding electric conductivity of graphene, the electrochemical response of the fabricated immunosensor was greatly enhanced and achieved the sensitive detection of HIgG. Meanwhile, the proposed electrochemical immunosensor also exhibited good precision, acceptable stability and reproducibility, and could be used for the detection of HIgG in real samples. Therefore, this novel dual amplified strategy opened a new door to broaden the potential applications of graphene in clinical research.

2. Experimental

2.1. Reagents and apparatus

Graphite powder (KS-10) and PDDA (20%) were from Sigma. *o*-Phenylenediamine (*o*-PD, 99%), H_2O_2 (30%), chloroauric acid and trisodium citrate were from Shanghai reagent Co. Inc. (Shanghai, China). Human IgG (HIgG) (Ag), rabbit anti-human IgG (Ab_1), HRP-labeled monoclonal goat anti-human IgG (HRP–Ab_2), HIgG enzyme-linked immunosorbent assay (ELISA) kits, bovine serum albumin (BSA), BCA protein assay kit and Tween-20 were purchased from Nanjing Keygen Co. Inc. (Nanjing, China). The clinical serum samples were kindly provided by the Gulou Hospital (Nanjing, China). The AuNPs solution used in all experiments were prepared according to the reported method by boiling $HAuC1_4$ aqueous solution with trisodium citrate (Enustun and Turkevich, 1963). The average diameter of the prepared AuNPs was about 20 nm.

Electrochemical measurements were performed on a CHI 660a workstation (Shanghai Chenhua, China) with a conventional three-electrode system comprised of a platinum wire auxiliary, a saturated calomel reference and the modified glass carbon (GCE) working electrode. The electrochemical impedance spectroscopy (EIS) analyses were performed with an Autolab PGSTAT12 (Eco chemie, BV, The Netherlands) in the solution of 0.10 M KNO_3 containing 10.0 mM $K_3[Fe(CN)_6]/K_4[Fe(CN)_6]$. UV–Vis spectra were obtained from a UV-3600 (Shimadzu) UV-Vis Spectrophotometers. HRTEM images were obtained on a JEOL 2100 high resolution transmission electron microscopy. Ultrasonication was performed using a KQ2200 ultrasonic cleaner (40 kHz, 100 W, China). Absorbance in BCA assay was recorded at 570 nm using Bio-Rad 680 microplate reader.

2.2. Preparation of AuNPs/PDDA-G hybrids

EGO dispersion was prepared from graphite according to a modified Hummer's method (Hummers and Offeman, 1958) and its concentration was estimated by calibration curve from the absorbance at 231 nm in the UV–Vis spectra. PDDA-G was prepared according to our previous work (Liu et al., 2010) and redispersed in water with a final concentration of 1.0 mg/mL. Furthermore, as a comparison, in a control experiment, pure graphene was also prepared by reduction of EGO using hydrazine without adding any stabilizer. Then, 2 mL of the as-prepared PDDA-G dispersion was added into 10 mL AuNPs solution (2.54×10^{-4} mol/L) and sonicated for 30 min. After centrifugation, the colorless supernatant was casted and the obtained AuNPs/PDDA-G composites were further washed with water for three times and redispersed in 4 mL water for further use.

2.3. Preparation of HRP–Ab_2/AuNPs/PDDA–EGO bioconjugates

EGO was functionalized with PDDA imitating previous literature (Cui et al., 2008b). 5 mL EGO dispersion (0.5 mg/mL) was mixed with 10 mL PDDA aqueous solution (1.0%) and sonicated for 30 min to give a homogeneous suspension. After centrifugation under 20,000 rpm, the complex was washed with water for at least three times and redispered in 5 mL water with mild sonication. To conjugate with AuNPs, 2 mL of the above PDDA–EGO dispersion was mixed with 5 mL AuNPs solution (2.54×10^{-4} mol/L) and sonicated for 30 min. After centrifugation, the colorless supernatant was discarded and the purple red AuNPs/PDDA–EGO composite was further washed with water for three times and redispered in 6 mL of 50 mM pH 9.0 Tris–HCl buffer solution. Finally, 100 μL HRP–Ab_2 (1 mg/mL) was added to 6.0 mL above AuNPs/PDDA–EGO composite solution and shaken overnight at room temperature. After centrifuged at 20,000 rpm, the obtained bioconjugate was further washed with buffer solution for at least three times and resuspended in 5.0 mL PBST (PBS, 0.05% Tween) that contained 0.1% BSA as the assay solution. The concentration of HRP–Ab_2 solution before and after assemble was measured by the BCA protein assay kit to quantify the loading amount of HRP–Ab_2 on the AuNPs/PDDA–EGO composite.

2.4. Immunoreaction and measurement procedure

The immunoassay procedure was illustrated in Scheme 1. Prior to use, the GCE with a diameter of 3 mm was successively polished using 0.3 and 0.05 μm alumina slurry followed by rinsing thoroughly with water. 5 μL AuNPs/PDDA-G composite solution was dropped on the pretreated GCE and allowed to dry at 4 °C overnight. Then the modified electrode was washed with PBST and immediately incubated with 50 μL of 0.1 mg/mL Ab_1 in pH 7.4 PBS for 12 h at 4 °C as the biomolecules could retain its bioactivity for a long time at this temperature. Next, they were rinsed with PBST to remove physically absorbed Ab_1 and blocked with 50 μL 2% BSA solution containing 0.05% Tween for 50 min at 37 °C to

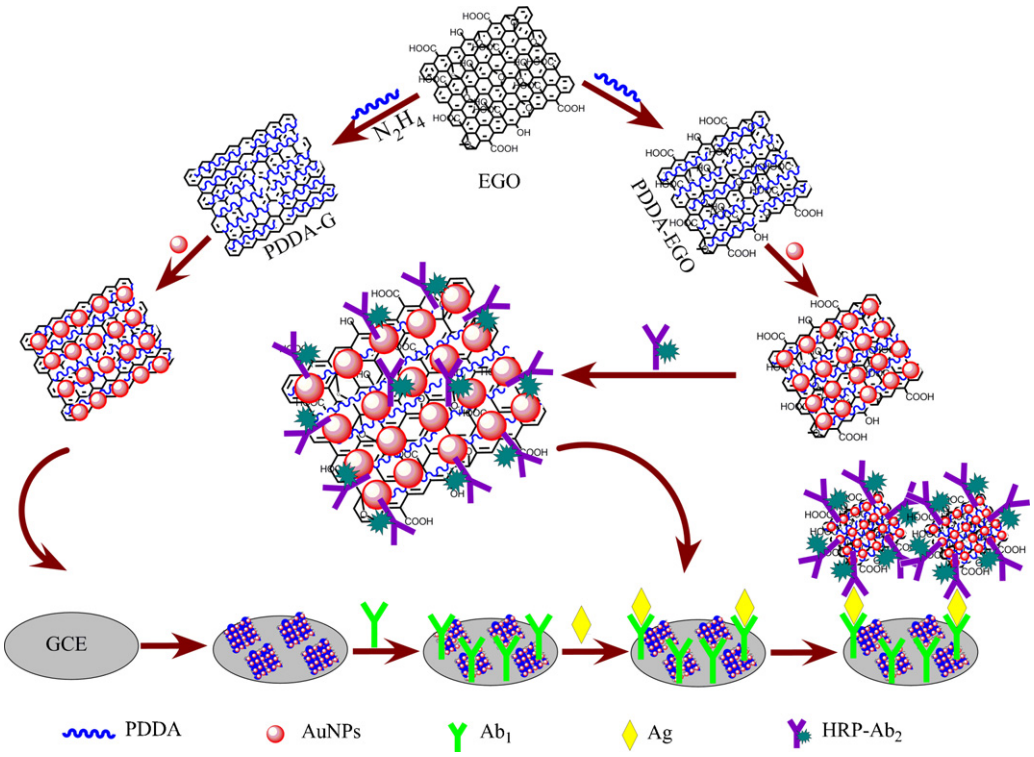

Scheme 1. Schematic illustration of the preparation of graphene-based hybrids and the construction of the sandwich-type electrochemical immunosensor.

block possible remaining active sites against non-specific adsorption. After washed with PBST, the Ab_1 modified electrode was incubated with 50 μL of the target HIgG antigen for 50 min at 37 °C as the immunoreaction could obtain higher efficiency at this temperature, and washed with PBST. Finally, the electrode was incubated with 50 μL of HRP–Ab_2/AuNPs/PDDA–EGO bioconjugate solution for 50 min at 37 °C and then washed thoroughly with PBST to remove non-specifically bounded conjugates. Electrochemical measurement was carried out in 5.0 mL of pH 7.0 PBS involving 2 mM *o*-PD and 4 mM H_2O_2 which was deaerated thoroughly with nitrogen before measurement and the differential pulse voltammetry (DPV) scan was performed from −0.3 to −0.8 V.

3. Results and discussion

3.1. Characterization of the composite

FT-IR spectroscopy was first used to investigate the reduction and the functionalization process as shown in Fig. S1. The dramatical decrease or disappearance of the adsorption bands of oxo-groups on pure graphene and the PDDA-G indicated that the EGO had been reduced successfully (Zhang et al., 2010; Shan et al., 2009b). Compared with PDDA, the peaks at 2930 cm^{-1} (CH_n), 1630 cm^{-1} (C═C) and 1430 cm^{-1} (C═C) in the spectra of PDDA-G clearly indicated the functionalization of graphene with PDDA (Yang et al., 2005). The images of water dispersion of graphene without and with PDDA in the inset of Fig. S1 show the good dispersity of PDDA-G. Additionally, as shown in the typical AFM images in Fig. S2, after reduction, the thickness of nanosheets increased to 1.3 nm of PDDA-G from 0.8 nm of EGO and each nanosheets kept independent in the dispersion due to the electrostatic interaction, which indicated that the PDDA played an important role as a capping reagent for the stabilization of the as-prepared PDDA-G nanosheets. Furthermore, Raman spectroscopy was also used to study the order and disorder structures of graphene (Reina et al., 2009; Hassan et al., 2009). As shown in Fig. S3, compared with graphite, the G band broadened and blue shifted to 1585 cm^{-1} accompanied with a significant increase of D band in EGO. The 2D band shape and the shift at 2681 cm^{-1} of PDDA-G indicated the single layer structure and the increase in thickness of PDDA-G should be attributed to the attachment of PDDA (Srinivas et al., 2010; Ferrari et al., 2006).

Next, to facilitate the immobilization for biomolecules to fabricate immunosensor, a novel AuNPs/PDDA-G hybrid architecture with good electric conductivity and biocompatibility was fabricated via a simple sonication-induced assembly. The obtained AuNPs/PDDA-G hybrid architecture was confirmed by the UV–Vis absorption spectrum as shown in Fig. 1A. The as-prepared citrate-stabilized colloidal AuNPs (curve a) appeared a strong characteristic absorption peak at 524 nm caused by surface plasmon resonance. PDDA-G (curve b) showed a strong absorption peak at 270 nm which referred to $\pi \rightarrow \pi^*$ transitions of aromatic C═C bond indicating the restoration of the π-conjugation network of the graphene nanosheets. Meanwhile, the band of $n \rightarrow \pi^*$ transition of C═O at about 300 nm was disappeared hinting the complete reduction of EGO (Zhou et al., 2009). After the AuNPs were deposited, the characteristic peak of AuNPs was observed in AuNPs/PDDA-G (curve c) at 526 nm which indicated the efficient adsorption of AuNPs onto the nanosheets surface. Additionally, the TEM image of the AuNPs/PDDA-G composite was also clearly indicated the formation of hybrid as shown in the inset of Fig. 1A. As could be seen, it clearly shows the thin flake-like shapes with some corrugation suggesting a flexible structure of the nanosheets and almost all anchored AuNPs were distributed homogeneously on the sheet surface with negligible nanoparticle agglomeration. Due to the upstanding electric conductivity of graphene and good biocompatibility of AuNPs, the AuNPs/PDDA-G composite could accelerate the electron transfer on the electrode surface and provided a biocompatible microenvironment for biomolecules loading as well as retaining native bioactivity. Therefore, it would be an ideal substrate material for electrode modification to immobilize biomolecules for immunoassay.

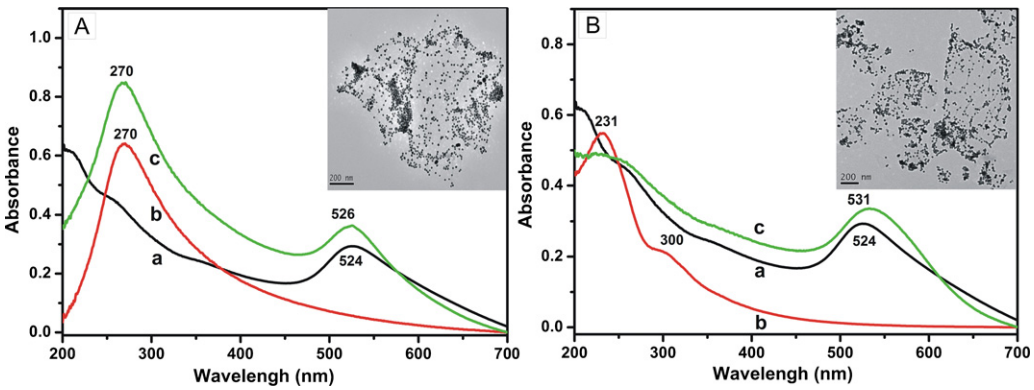

Fig. 1. (A) UV–Vis absorption spectra of AuNPs (a), PDDA-G (b) and AuNPs/PDDA-G (c). Inset: TEM image of AuNPs/PDDA-G. (B) UV–Vis absorption spectra of AuNPs (a), EGO (b), AuNPs/PDDA–EGO (c). Inset: TEM image of AuNPs/PDDA–EGO.

Furthermore, for the signal amplification to improve the sensitivity of immunosensor, EGO was selected to conjugate with AuNPs to obtain AuNPs/PDDA–EGO composite for the labeling of enzyme label-antibody. The UV–Vis absorption spectrum was also used to confirm the formation of the composite as shown in Fig. 1B. As could be seen, the EGO (curve b) showed a strong absorption peak at 231 nm and a shoulder peak at 300 nm, which corresponded to $\pi \rightarrow \pi^*$ transitions of aromatic C=C bond and $n \rightarrow \pi^*$ transition of C=O bond, respectively (Chen and Yan, 2010). After decorated with AuNPs, AuNPs/PDDA–EGO showed a characteristic peak of AuNPs at 531 nm which indicated the capture of AuNPs. The slight red shift of resonance wavelength of AuNPs in the hybrid attributed to interparticle plasmon coupling as observed in clustered AuNPs (Guarise et al., 2005; Thomas et al., 2004), which suggested that the surface-modified AuNPs tightly stacked with each other but without agglomeration, as evidenced by the TEM images in the inset of Fig. 1B. As could be seen, the sheets remained separated with each other without any aggregation indicating the high soluble dispersity of PDDA–EGO and all AuNPs absorbed homogeneously on the sheet surface same as the AuNPs/PDDA-G. Owing to the large special surface areas of EGO and the good affinity of AuNPs to biomolecules, the AuNPs could be deposited on both sides of PDDA–EGO sheets and it was beneficial to increase the loading amount of enzyme label-antibody.

Finally, a novel bioconjugate of HRP–Ab_2/AuNPs/PDDA–EGO was first developed for multilabel signal amplification to enhance sensitivity via adsorption of HRP–Ab_2 on the surface of AuNPs/PDDA–EGO through the interaction between AuNPs and mercapto or primary amine groups of biomolecules (Hayat, 1989; Xu, 1997). The amount of HRP–Ab_2 adsorbed onto the AuNPs/PDDA–EGO composites was determined through the measurement of protein concentration in supernatant before and after the adsorption through a BCA protein assay which was a typical measurement method for protein concentration (Hill and Straka, 1988). Then, the total amount of HRP–Ab_2 in the stock HRP–Ab_2/AuNPs/PDDA–EGO dispersion (5 mL with EGO concentration of 0.5 mg/mL) was estimated to be 16.82 μg.

3.2. Electrochemical behavior of the immunosensor

EIS was an effective technique for probing the surface features of modified electrodes to understand the chemical transformations and processes associated with the conductive electrode surface. The impedance spectra include a semicircle portion and a linear portion. The semicircle diameter at higher frequencies corresponds to the electron-transfer resistance (R_{et}), and the linear part at lower frequencies corresponds to the diffusion process. The stepwise construction process of the immunosensor was characterized by EIS as shown in Fig. 2A. The bare GCE (curve a) displayed a small semicircle with a R_{et} of about 90 Ω at high frequencies. After the bare electrode was modified with AuNPs/PDDA-G composite film, the electrode showed a much lower resistance for the redox probe (curve b), implying that AuNPs/PDDA-G was an excellent electric conducting material and accelerated the electron transfer. Subsequently, when the Ab_1 was loaded on the surface of AuNPs/PDDA-G modified electrode, the R_{et} increased which suggested that the Ab_1 formed an additional barrier and further prevented the redox probe to the electrode surface (curve c). This result was consistent with the fact that the hydrophobic layer of protein insults the conductive support and hinders the interfacial electron transfer. After the electrode was incubated with BSA to block non-specific sites of electrode surface, the R_{et} increased significantly to about 230 Ω (curve d). Furthermore, the R_{et} reached to about 300 Ω after bounded with Ag (curve e), then to about 330 Ω after incubated with HRP–Ab_2 (curve f) which indicates the formation of hydrophobic immunocomplex layer embarrassing the electron transfer.

The amperometric response of the sensor was shown in Fig. 2B. No obvious response was observed at both bare GCE (curve a) and Ag/BSA/Ab_1/AuNPs/PDDA-G modified GCE (curve b) over the working potential range in 0.1 M pH 7.0 PBS containing 2 mM *o*-PD and 4 mM H_2O_2. After incubated with conventional HRP–Ab_2, a pair of stable and well defined redox peaks was observed at the HRP–Ab_2/Ag/BSA/Ab_1/AuNPs/PDDA-G modified GCE (curve c) at −0.632 V and −0.566 V corresponding to the redox of enzymatic product of 2, 3-diaminophenazine. However, when incubated with HRP–Ab_2/AuNPs/PDDA–EGO bioconjugate, the redox peaks of enzymatic product increased significantly compared to the HRP–Ab_2/Ag/BSA/Ab_1/AuNPs/PDDA-G modified GCE at the obtained HRP–Ab_2/AuNPs/PDDA–EGO bioconjugate/Ag/BSA/Ab_1/AuNPs/PDDA-G modified GCE (curve d). This phenomenon indicated that the AuNPs/PDDA–EGO hybrid provided a large number of active sites which could increase the loading amount of HRP–Ab_2 in the enzymatic reaction to develop the sensitivity of immunoassay.

3.3. Performance of the immunosensor

In order to investigate the analytical performance of the obtained immunosensor, differential pulse voltammetrics (DPV) was explored for the amperometric response of HIgG at the immunosensor. Fig. 3A shows the typical DPV obtained after the sandwich immunoreactions for different concentrations of HIgG using HRP–Ab_2/AuNPs/PDDA–EGO bioconjugates as the label. In a controlled experiment, the sensor was performed through the full procedure without exposure to antigen, and the final electrode still

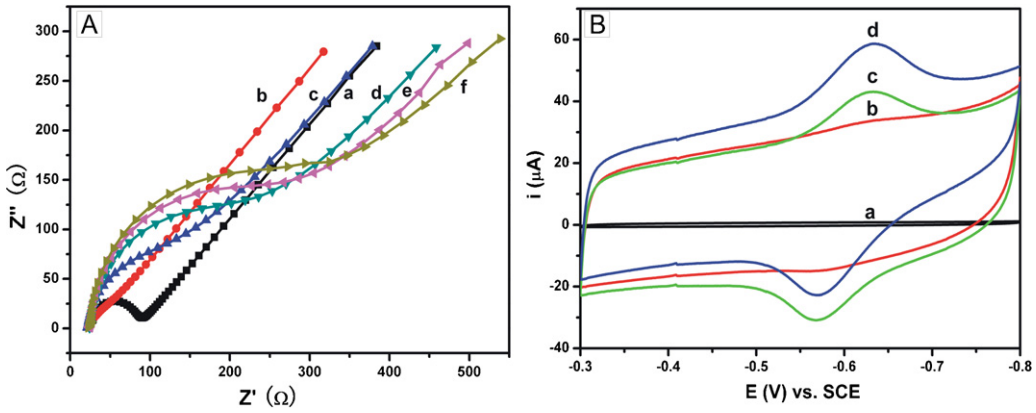

Fig. 2. (A) EIS of bare (a), AuNPs/PDDA-G (b), Ab_1/AuNPs/PDDA-G (c), BSA/Ab_1/AuNPs/PDDA-G (d), Ag/BSA/Ab_1/AuNPs/PDDA-G (e) and HRP–Ab_2/Ag/BSA/Ab_1/AuNPs/PDDA-G (f) modified GCEs in 0.10 M KNO_3 containing 10.0 mM $K_3[Fe(CN)_6]/K_4[Fe(CN)_6]$. (B) CVs of GCE (a), Ag/BSA/Ab_1/AuNPs/PDDA-G/GCE (b), HRP–Ab_2/Ag/BSA/Ab_1/AuNPs/PDDA-G/GCE (c) and HRP–Ab_2/AuNPs/PDDA-EGO bioconjugate/Ag/BSA/Ab_1/AuNPs/PDDA-G/GCE in 0.1 M pH 7.0 PBS containing 2 mM *o*-PD and 4 mM H_2O_2.

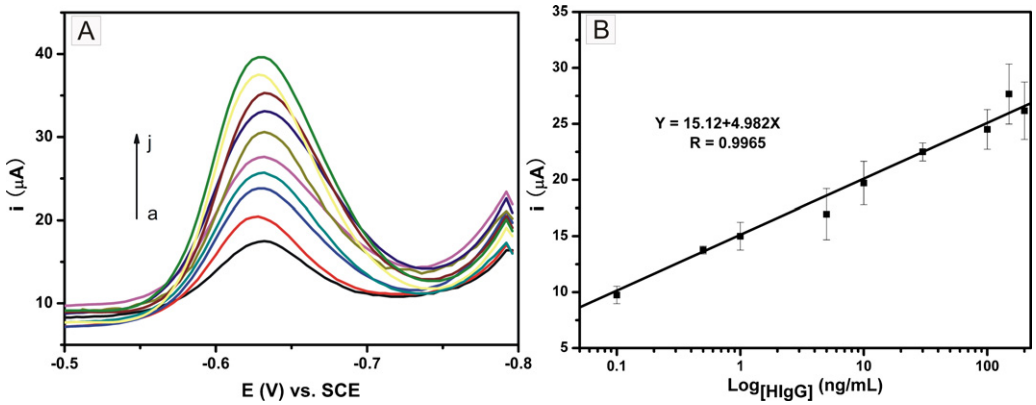

Fig. 3. (A) Typical DPV of immunosensor using HRP–Ab_2/AuNPs/PDDA–EGO bioconjugate as label with increasing HIgG from a to j (0, 0.1, 0.5, 1.0, 5.0, 10.0, 30.0, 100.0, 150.0, 200.0 ng/mL) in 0.1 M pH 7.0 PBS containing 2 mM *o*-PD and 4 mM H_2O_2. (B) Calibration curve of the immunosensor for HIgG determination plotted on a semi-log scale.

behaved a conspicuous peak in 0.1 M pH 7.0 PBS containing 2 mM *o*-PD and 4 mM H_2O_2 (curve a), which might be caused by the physical adsorption of the HRP–Ab_2/AuNPs/PDDA–EGO bioconjugates on the GCE. However, the DPV signals were obviously enhanced in the presence of antigen. Under optimal conditions, the peak currents had a good linear relationship with the logarithm of HIgG concentration from 0.1 to 200 ng/mL as shown in Fig. 3B. The linear regression equation was $i(\mu A) = 15.12 + 4.98 \log C_{HIgG}$ (ng/mL) with a correlation coefficient (R) of 0.9965. The detection limit ($S/N = 3$) was estimated to be about 0.05 ng/mL.

As a comparison, the amperometric response of conventional HRP–Ab_2 label was also investigated as shown in Fig. 4. Under the same conditions, the signal intensity was greatly decreased compared with the HRP–Ab_2/AuNPs/PDDA–EGO label at different concentrations of HIgG. Meanwhile, the catalytic current on HRP–Ab_2/AuNPs/PDDA–EGO labeled electrode was greatly enhanced compared with the blank (with HIgG concentration of 0 ng/mL). This result indicated that the analysis sensitivity greatly enhanced using HRP–Ab_2/AuNPs/PDDA–EGO bioconjugates as label which was a result of a higher number of HRP molecules loaded on the AuNPs/PDDA–EGO hybrid to achieve the signal amplification. Therefore, the proposed immunosensor exhibited a good analytical performance for the HIgG detection and could be used for the detection of HIgG in real sample.

Furthermore, the analytical performance of the proposed immunosensor had been compared with that of other HIgG immunosensors reported. As shown in Table S1, the present sensor displayed a good performance than some earlier reported methods, especially the detection limit.

3.4. Specificity, reproducibility and stability of the immunosensor

The specificity of the immunosensor played an important role in analyzing biological samples *in situ* without separation. Some proteins such as C-reactive protein (CRP), carcinoembryonic antigen (CEA) and α-fetoprotein (AFP) were used as the interfere to evaluate the specificity through comparing the electrochemical responses of 100 ng/mL pure HIgG and a same solution containing additional interfere of 500 ng/mL. The currents response changes were 6.2%, 5.5% and 8.7%, respectively, which indicated that the specificity of the immunosensor was acceptable. The intra-assay precision was estimated by testing one HIgG level for five replicate measurements. The inter-assay precision or the fabrication reproducibility was also estimated by measuring one HIgG level with five immunosensors made at the same GCE independently. The relative standard deviations of the intra- and inter-assay were 9.3% and 9.7%, respectively, at the HIgG concentration of 100 ng/mL. This result indicated that the immunosensor possessed acceptable precision and reproducibility. Furthermore, when the immunosensor was stored at 4 °C for 20 days, it retained 91.0% of its response, indicating the good stability of the immunosensor which attributed to the strong interactions between the AuNPs/PDDA-G and Ab_1. The slow decrease of response might be due to the gradual deactivation of the immobilized biomolecules.

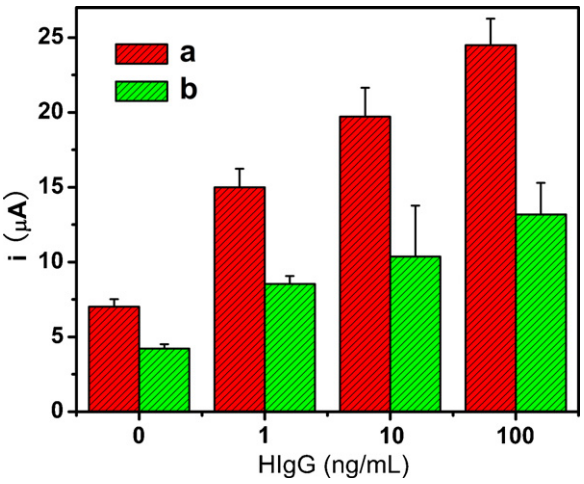

Fig. 4. Comparison of amperometric response between HRP–Ab_2/AuNPs/PDDA–EGO bioconjugate/Ag/BSA/Ab_1/AuNPs/PDDA-G/GCE (a) and HRP–Ab_2/Ag/BSA/Ab_1/AuNPs/PDDA-G/GCE (b) at different concentrations of HIgG (0, 1, 10 and 100 ng/mL) in 0.1 M pH 7.0 PBS containing 2 mM *o*-PD and 4 mM H_2O_2.

Table 1
Comparison of serum HIgG levels determined using two methods.

Serum samples	1	2	3
Immunosensor (ng/mL)[a]	90.65	9.72	1.93
ELISA (ng/mL)[a]	97.02	9.01	2.00
Relative deviation (%)	−6.57	7.89	−3.50

[a] The average value of three successive determinations.

3.5. Application of the immunosensor in human serum

The feasibility of applying the immunosensor in clinical systems was investigated via analyzing several real clinical serum samples, and the results were then compared with the reference values obtained by the commercial ELISA method. Table 1 shows the correlation results obtained using the proposed immunosensor and the ELISA method. The relative deviations of the proposed immunosensor ranged from −3.50% to 7.89%. It obviously suggested that there was no significant difference between the results given by two methods. Therefore, the proposed sensor could be reasonably applied in the clinical determination of HIgG in human plasma.

4. Conclusion

In summary, PDDA-G were successfully prepared by a simple synthetic method and decorated with AuNPs. The obtained AuNPs/PDDA-G hybrid architecture could be an ideal substrate for antibody immobilization with good stability and bioactivity. Furthermore, multilabel-antibody functionalized EGO composites were also prepared and applied as labels in sandwich electrochemical immunoassay. Due to the dual signal amplification strategy of graphene-based architecture and the multilabel, the electrochemical response of the fabricated immunosensor was greatly enhanced and achieved the sensitive detection of HIgG. Meanwhile, the proposed electrochemical immunosensor also exhibited good precision, acceptable stability and reproducibility, and could be used for the detection of HIgG in real serum samples. Therefore, this novel dual amplified strategy opened a new door to broaden the potential applications of graphene in clinical research.

Acknowledgments

The authors acknowledge the support of National Natural Science Foundation of China (Nos. 20821063 and 20775030). This work is also supported by 973 Program (No: 2011CB933502).

Appendix A. Supplementary data

Supplementary data associated with this article can be found, in the online version, at doi:10.1016/j.bios.2011.02.018.

References

Bilitewski, U., 2000. Anal. Chem. 72, 692A–701A.
Chen, J.L., Yan, X.P., 2010. J. Mater. Chem. 20, 4328–4332.
Cui, R.J., Liu, C., Shen, J.M., Gao, D., Zhu, J.J., Chen, H.Y., 2008a. Adv. Funct. Mater. 18, 2197–2204.
Cui, R.J., Huang, H.P., Yin, Z.Z., Gao, D., Zhu, J.J., 2008b. Biosens. Bioelectron. 23, 1666–1673.
Dreyer, D.R., Park, S., Bielawski, C.W., Ruoff, R.S., 2010. Chem. Soc. Rev. 39, 228–240.
Du, D., Zou, Z.X., Shin, Y., Wang, J., Wu, H., Engelhard, M.H., Liu, J., Aksay, I.A., Lin, Y.H., 2010a. Anal. Chem. 82, 2989–2995.
Du, M., Yang, T., Jiao, K., 2010b. J. Mater. Chem. 20, 9253–9260.
Enustun, B.V., Turkevich, J., 1963. J. Am. Chem. Soc. 85, 3317–3328.
Ferrari, A.C., Meyer, J.C., Scardaci, V., Casiraghi, C., Lazzeri, M., Mauri, F., Piscanec, S., Jiang, D., Novoselov, K.S., Roth, S., Geim, A.K., 2006. Phys. Rev. Lett. 97, 187401.
Geim, A.K., Novoselov, K.S., 2007. Nat. Mater. 6, 183–191.
Guarise, C., Pasquato, L., Scrimin, P., 2005. Langmuir 21, 5537–5541.
Hansen, J.A., Mukhopadhyay, R., Hansen, J., Gothelf, K.V., 2006. J. Am. Chem. Soc. 128, 3860–3861.
Hassan, H.M.A., Abdelsayed, V., Khder, A.E.R.S., AbouZeid, K.M., Terner, J., El-Shall, M.S., Al-Resayes, S.I., El-Azhary, A.A., 2009. J. Mater. Chem. 19, 3832–3837.
Hayat, M.A., 1989. Colloidal Gold: Principles, Methods and Applications. Academic Press, New York.
Hill, H.D., Straka, J.G., 1988. Anal. Biochem. 170, 203–208.
Hummers, W.S., Offeman, R.E., 1958. J. Am. Chem. Soc. 80, 1339.
Kato, K., Shimizu, A., 1986. Clin. Chim. Acta 158, 99–108.
Li, D., Müller, M.B., Gilje, S., Kaner, R.B., Wallace, G.G., 2008. Nat. Nanotechnol. 3, 101–105.
Li, X.L., Yuan, R., Chai, Y.Q., Zhang, L.Y., Zhuo, Y., Zhang, Y., 2006. J. Biotechnol. 123, 356–366.
Lin, J.H., Yan, F., Ju, H.X., 2004. Clin. Chim. Acta 341, 109–115.
Liu, K.P., Zhang, J.J., Yang, G.H., Wang, C.M., Zhu, J.J., 2010. Electrochem. Commun. 12, 402–405.
Liu, Z., Robinson, J.T., Sun, X.M., Dai, H.J., 2008. J. Am. Chem. Soc. 130, 10876–10877.
Lv, W., Guo, M., Liang, M.H., Jin, F.M., Cui, L., Zhi, L.J., Yang, Q.H., 2010. J. Mater. Chem. 20, 6668–6673.
Novoselov, K.S., Geim, A.K., Morozov, S.V., Jiang, D., Katsnelson, M.I., Grigorieva, I.V., Dubonos, S.V., Firsov, A.A., 2005. Nature 438, 197–200.
Reina, A., Jia, X.T., Ho, J., Nezich, D., Son, H., Bulovic, V., Dresselhaus, M.S., Kong, J., 2009. Nano Lett. 9, 30–35.
Rijiravanich, P., Somasundrum, M., Surareungchai, W., 2008. Anal. Chem. 80, 3904–3909.
Shan, C.S., Yang, H.F., Song, J.F., Han, D.X., Ivaska, A., Niu, L., 2009a. Anal. Chem. 81, 2378–2382.
Shan, C.S., Yang, H.F., Han, D.X., Zhang, Q.X., Ivaska, A., Niu, L., 2009b. Langmuir 25, 12030–12033.
Srinivas, G., Zhu, Y., Piner, R., Skipper, N., Ellerby, M., Ruoff, R., 2010. Carbon 48, 630–635.
Stankovich, S., Piner, R.D., Chen, X.Q., Wu, N.Q., Nguyen, S.T., Ruoff, R.S., 2006. J. Mater. Chem. 16, 155–158.
Tang, D.P., Su, B.L., Tang, J., Ren, J.J., Chen, G.N., 2010. Anal. Chem. 82, 1527–1534.
Thomas, K.G., Barazzouk, S., Ipe, B.I., Joseph, S.T.S., Kamat, P.V., 2004. J. Phys. Chem. B 108, 13066–13068.
Van Emon, J.M., Lopez-Avila, V., 1992. Anal. Chem. 64, 78A–88A.
Wang, J., 2006. Biosens. Bioelectron. 21, 1887–1892.
Wei, Q., Xin, X.D., Du, B., Wu, D., Han, Y.Y., Zhao, Y.F., Cai, Y.Y., Li, R., Yang, M.H., Li, H., 2010. Biosens. Bioelectron. 26, 723–729.
Wu, Y.F., Chen, C.L., Liu, S.Q., 2009. Anal. Chem. 81, 1600–1607.
Xia, F.N., Farmer, D.B., Lin, Y.M., Avouris, P., 2010. Nano Lett. 10, 715–718.
Xu, Y.W., 1997. Detection Techniques in Immunology. Science Press, Beijing.
Yang, D.Q., Rochette, J.F., Sacher, E., 2005. Phys. Chem. B 109, 4481–4484.
Yu, X., Munge, B., Patel, Y., Jensen, G., Bhirde, A., Gong, J.D., Kim, S.N., Gillespie, J., Gutkind, J.S., Papadimitrakopoulos, F., Rusling, J.F., 2006. J. Am. Chem. Soc. 128, 11199–11205.
Zhang, H., Lv, X.J., Li, Y.M., Wang, Y., Li, J.H., 2010. ACS Nano 4, 380–386.
Zhang, X.N., Geng, P., Liu, H.J., Teng, Y.Q., Liu, Y.J., Wang, Q.J., Zhang, W., Jin, L.T., Jiang, L., 2009. Biosens. Bioelectron. 24, 2155–2159.
Zhou, Y., Bao, Q.L., Tang, L.A.L., Zhong, Y.L., Loh, K.P., 2009. Chem. Mater. 21, 2950–2956.